Open access • Journal Article • DOI:10.1088/0029-5515/31/9/002

An investigation of beam driven alfvén instabilities in the diii-d tokamak

William Heidbrink, E. J. Strait, E. J. Doyle, G. Sager ...+1 more authors

Institutions: University of California, Irvine, University of California, Los Angeles, University of Illinois at Urbana–Champaign

Published on: 01 Sep 1991 - Nuclear Fusion (IOP Publishing)

Topics: Beam (structure) and DIII-D

AN INVESTIGATION OF BEAM DRIVEN ALFVÉN INSTABILITIES IN THE DIII-D TOKAMAK

W.W. HEIDBRINK*, E.J. STRAIT, E. DOYLE**,
G. SAGER***, R.T. SNIDER
General Atomics,
San Diego, California,
United States of America

ABSTRACT. Neutral beams were injected into low field (B = 0.7–1.0 T) deuterium plasmas in an attempt to destabilize toroidicity induced Alfvén eigenmodes (TAE modes). When the parallel beam velocity approached the Alfvén velocity and the volume averaged beam beta exceeded 2%, localized, propagating modes with n = 2–10 were observed. As much as 45% of the beam power was lost as a result of the modes. The threshold for TAE instability is at least one order of magnitude higher than that predicted by Fu and VanDam (Phys. Fluids B 1 (1989) 1949).

1. INTRODUCTION

To sustain ignition in a tokamak reactor, most of the alpha particles produced in D-T fusion reactions must thermalize in the plasma. If the energetic alpha population drives collective instabilities that result in anomalous losses of the alphas, the reactor will not ignite. Therefore, it is desirable, before construction of a reactor, to assess the likelihood that alphas will drive collective instabilities. In this paper, we describe experiments in which neutral beam injection is employed to create an energetic ion population that simulates the alphas. The principal difference between a beam population and an alpha population in a reactor is that the distribution of beam ions is anisotropic in velocity space (the alpha distribution is isotropic). In other regards, the beam ion distribution effectively simulates alpha physics in a 20 kV reactor such as the International Thermonuclear Experimental Reactor (ITER) (Table I). Our experiments are also relevant to neutral beam current drive with ~1 MeV ions in future devices such as ITER [1]. If Alfvén instabilities cause appreciable anomalous losses or pitch angle scattering of the circulating beam ions, the current drive efficiency will be reduced and a high plasma current will not be sustained. Finally, destabilization of Alfvén waves by energetic ions is of fundamental interest, since super-Alfvénic ion populations are common in space [2].

Destabilization of shear Alfvén waves by circulating fast ions has been explored theoretically by many authors. In a homogeneous plasma, Alfvén waves are normal modes of the plasma that are weakly Landau damped by electrons. The waves are analogous to transverse waves on a string and propagate with a phase velocity $\omega/k_\parallel \simeq v_A = B/\sqrt{4\pi n_i m_i}$, where the 'tension' of the string is provided by the magnetic field B and the 'inertia' of the string is due to the ion mass density $n_i m_i$. For instability, the waves must gain enough energy from the fast ion distribution to overcome electron damping. Fast ion distributions that are non-monotonic in velocity space ($\partial F/\partial v_\parallel^2 > 0$) can be unstable through inverse Landau damping [3]. Although these velocity space instabilities might be observed transiently, steady state slowing down distributions generally are monotonic in velocity space and thus configuration space instabilities are of greater concern.

TABLE I. COMPARISON OF BEAM IONS IN DIII-D AND ALPHAS IN ITER

Ratio	Description	DIII-D	ITER [1]
$\rho_f:\rho_i:\rho_e$	Gyroradii of fast ions, thermal ions and electrons	6:1:0.16	10:1:0.16
$v_e:v_f:v_i$	Velocities of electrons, fast ions and thermal ions	10:1:0.16	6:1:0.26
$\beta_f(0)$	Central fast ion pressure to magnetic field pressure	≤15%	2–4%
$v_\parallel/v_A$	Fast ion velocity to Alfvén velocity	≤1.4	1.9

Permanent addresses:
* Physics Department, University of California, Irvine, CA, USA.
** Electrical Engineering Department, University of California, Los Angeles, CA, USA.
*** Nuclear Engineering Department, University of Illinois, Urbana, IL, USA.

Because of the curvature drift in toroidal geometry, circulating fast ions can resonate with Alfvén waves on different mode rational surfaces [4]. This provides a mechanism to tap the free energy in the fast ion pressure gradient. These so-called kinetic Alfvén waves (KAW) have radial eigenfunctions that are localized near rational surfaces. A necessary condition for KAW instability is that the beam parallel velocity exceed the Alfvén velocity $v_\parallel/v_A > 1$. In contrast, global Alfvén eigenmodes (GAE) have radial eigenfunctions that span most of the plasma [5]. Some eigenmodes have phase velocities below the Alfvén velocity and can therefore resonate with beam ions of velocity as low as $v_\parallel/v_A \simeq 0.5$ [6]. Both the fast ion population and the plasma current distribution affect GAE stability. Recent calculations [7, 8] suggest that toroidal effects will stabilize these modes in a reactor. Another class of Alfvén waves with globally extended eigenfunctions are the toroidicity induced Alfvén eigenmodes (TAE) [9]. These modes arise owing to toroidal coupling between cylindrical modes. Because the eigenfunction peaks between rational surfaces, electron damping is predicted to be smaller than for kinetic Alfvén waves and the calculated stability threshold is lower [10, 11]. A radially peaked beam profile and $v_\parallel/v_A \gtrsim 1$ are necessary for TAE instability [12]. Recent calculations predict that alphas will drive low n (n is the toroidal mode number) TAE modes unstable in a reactor [10, 12, 13] and that extremely rapid diffusion of alphas will occur [14].

Intense neutral beam injection has been studied on numerous tokamaks, but super-Alfvénic populations have been created relatively rarely. In the T-11 tokamak, plasmas with $v_\parallel/v_A \simeq 2$ exhibited large voltage spikes [15]. In Doublet III, fast ion losses were observed when $v_\parallel/v_A \simeq 1.3$, but the results may have been due to prompt orbit losses [16]. Low frequency instabilities were observed in ISX-B [17] and JFT-2 [18] plasmas with $v_\parallel/v_A \simeq 1$. Measurements of fluctuations in the Alfvén range of frequencies (50–1000 kHz) were not performed in these previous experiments. Beam driven instabilities with frequencies >50 kHz were observed previously on PDX [19] and PBX [20], but the beam ion populations were sub-Alfvénic. Concurrently with our study, Wong et al. [21] reported the observation of TAE modes in TFTR.

This paper and the recent paper from PPPL [21] report the first detailed studies of fast ion driven Alfvén instabilities in a tokamak. Since it can operate with small values of the Alfvén velocity and is equipped with intense neutral beam injectors, the DIII-D facility is well suited for studies of Alfvén instabilities (Section 2). Instability was only observed [22] when the parallel beam velocity was close to the Alfvén velocity and when the beam beta ($\gtrsim 2\%$) and the normalized beta ($\beta_n \equiv \beta_t aB/I \gtrsim 3.2$) were large (Section 3). The observed modes may be toroidicity induced Alfvén eigenmodes (Section 4). The threshold for TAE instability is at least one order of magnitude larger than predicted by simple analytic formulas (Section 5).

2. APPARATUS

An approximate expression for the growth rate of TAE instability [10] is

$$\frac{\gamma}{\omega} \simeq \frac{9}{4}\left[\beta_f\left(\frac{\omega_{*f}}{\omega} - \frac{1}{2}\right)F - \beta_e\frac{v_A}{v_e}\right] \qquad (1)$$

where β_f and β_e are the local fast ion and electron beta, respectively, $\omega_{*f} = -(m/r)(c/n_f e_f B)(dp_f/dr)$ is the fast ion diamagnetic frequency (m is the poloidal mode number, e_f, n_f and p_f are the fast ion charge, density and pressure, respectively, and r is the minor radius), F is proportional to the fraction of the fast ion distribution function that resonates with the mode, and the mode frequency ω is approximately $v_A/2qR$. Equation (1) states that the beam drive (the first term on the RHS) is opposed by electron damping (the second term on the RHS). The beam drive is enhanced by large beam beta (β_f), by a steep beam pressure gradient (ω_{*f}), and by a distribution function with many resonant particles (F). The wave particle resonance condition is $v_\parallel = v_A/(2|m - nq|)$ [12]. Since the eigenfunction for a gap mode peaks near $q = \left(m + \frac{1}{2}\right)/n$, this implies that the beam ions must be nearly super-Alfvénic ($v_\parallel \simeq v_A$) for instability. The electron damping term depends weakly on plasma temperature ($\propto \sqrt{T_e}$).

In terms of experimental operation, Eq. (1) suggests the following prescription for Alfvén instability:

- Minimize the toroidal field to maximize β_f and minimize v_A;
- Maximize the parallel beam velocity and beam power;
- Maximize the plasma mass-to-charge ratio to minimize v_A;
- Use low to moderate plasma density; low density increases β_f by reducing the slowing down time and tends to minimize β_e; high density minimizes v_A;
- Obtain peaked profiles to maximize the beam density gradient.

DIII-D [23] is well suited for Alfvén instability studies. Its low aspect ratio ($a \simeq 65$ cm; major radius

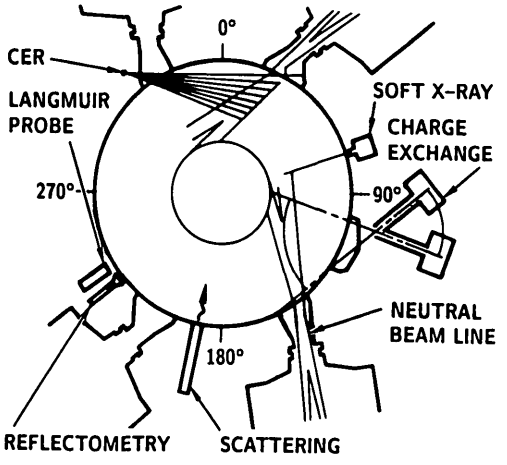

FIG. 1. Plan view of the DIII-D tokamak. Eight neutral beam sources housed in four beam boxes inject neutrals in the direction of the plasma current. Active charge exchange measurements are obtained by modulating one of the heating beams at 150°. The neutral deposition is measured by the CER diagnostic that views the nominally identical beam at 30°. Fluctuation diagnostics include SXR cameras, a laser scattering diagnostic, microwave reflectometry, a midplane Langmuir probe and numerous Mirnov coils (not shown).

$R_0 \simeq 167$ cm) and elongation ($\kappa \simeq 2.0$) permit low toroidal field ($\lesssim 1.0$ T), moderate density ($\bar{n}_e \sim 5 \times 10^{13}$ cm^{-3}), moderate current (~ 1 MA) operation without encountering density or q limits. Its neutral beams are intense ($\lesssim 20$ MW), energetic ($\lesssim 80$ kV) and fairly tangential (half of the sources inject at a tangency radius $R_{tan} = 74$ cm and half of them inject at $R_{tan} = 110$ cm) (Fig. 1). The neutral beams can be operated in either hydrogen or deuterium. For 75 kV beam ions with $R_{tan} = 110$ cm that ionize on axis, the ratio of initial parallel velocity $v_{\|0} \equiv R_{tan} v_0 / R_0$ to Alfvén velocity v_A is

$$\frac{v_{\|0}}{v_A} = \frac{0.53}{B_T} \sqrt{\frac{n_{13}}{A_b}\left(1 - \frac{n_H}{2n_e}\right)} \qquad (2)$$

where n_{13} is the electron density in units of 10^{13} cm^{-3}, B_T is the magnetic field in T, n_H/n_e is the hydrogen concentration and A_b is the beam atomic mass. For hydrogen injection ($A_b = 1$), super-Alfvénic populations are readily obtained, while, for deuterium injection, $v_{\|0}/v_A \lesssim 1$. However, the beam beta β_f is much smaller for hydrogen injection than for deuterium injection, since the beam power is smaller and the beam ion slowing down time τ_s is shorter (owing to the mass dependence of τ_s and the poorer confinement (lower T_e) generally obtained with $H^0 \rightarrow D^+$). In all the experiments reported here, deuterium fill gas was used to maximize $n_i m_i$. For the $H^0 \rightarrow D^+$ experiments, helium glow discharge cleaning, followed by deuterium discharge cleaning, was employed after each discharge to minimize the concentration of hydrogen in the plasma.

The principal fluctuation diagnostics (Fig. 1) were soft X-ray (SXR) camera arrays [24] and extensive arrays of electrostatically shielded Mirnov coils. For this study, a poloidal array of 25 Mirnov loops (typically spaced 10–20° apart) and a toroidal array of eight loops near the outboard midplane (with a variable spacing of 6–90°) were employed. In principle, these arrays allow poloidal mode numbers $m \lesssim 20$ and toroidal mode numbers $n \lesssim 30$ to be detected. The electronics of the SXR diagnostic passes signals up to 750 kHz. Data from both diagnostics were archived at 500 kHz. A multichannel microwave reflectometer system [25] monitored density fluctuations between 0 and 400 kHz for cut-off layers below $\sim 2 \times 10^{13}$ cm^{-3}, which corresponded to the plasma edge for these experiments. The far-infrared (FIR) scattering system [26] was tuned to $k = 2.5$ cm^{-1} and $k = 5.0$ cm^{-1} to maximize the likelihood of detecting the relatively long wavelength Alfvén waves. For these small values of k, the scattering volume encompassed most of the plasma cross-section. Frequencies up to 1 MHz were monitored. Spectra from a floating Langmuir probe situated ~ 1.4 cm behind the graphite tiles in the horizontal midplane were obtained with a spectrum analyser that swept between 100 kHz and 1 MHz every ~ 120 ms. A DC break between the probe and the spectrum analyser restricted the sensitivity of this diagnostic to frequencies above ~ 300 kHz.

The behaviour of the fast ions was diagnosed using neutron scintillators during deuterium injection and active charge exchange during hydrogen injection. The neutron diagnostic [19, 27] has a maximum frequency response of ~ 20 kHz. For these experiments, the charge exchange detector [28] was usually oriented to intersect a heating beam near the centre of the plasma ($R \simeq 169$ cm) at a pitch angle ($\chi \equiv \cos^{-1}(v_\|/v) = 35°$) close to the angle of injection of the more tangential beams. The heating beam was turned off for 10 ms every 50 ms in order to measure the 'background' signal from passive charge exchange and noise; the difference between the charge exchange signal when the beam is on and when it is off is the 'active' signal from the volume where the charge exchange sightline intersects the heating beam. Note that, since the beam slowing down time was ~ 45 ms in our $H^0 \rightarrow D^+$ plasmas, the beam ion population scarcely changed during the 10 ms in which one of the beams was turned off. For deuterium injection, interference associated with 2.5 MeV neutrons prevented valid charge exchange measurements.

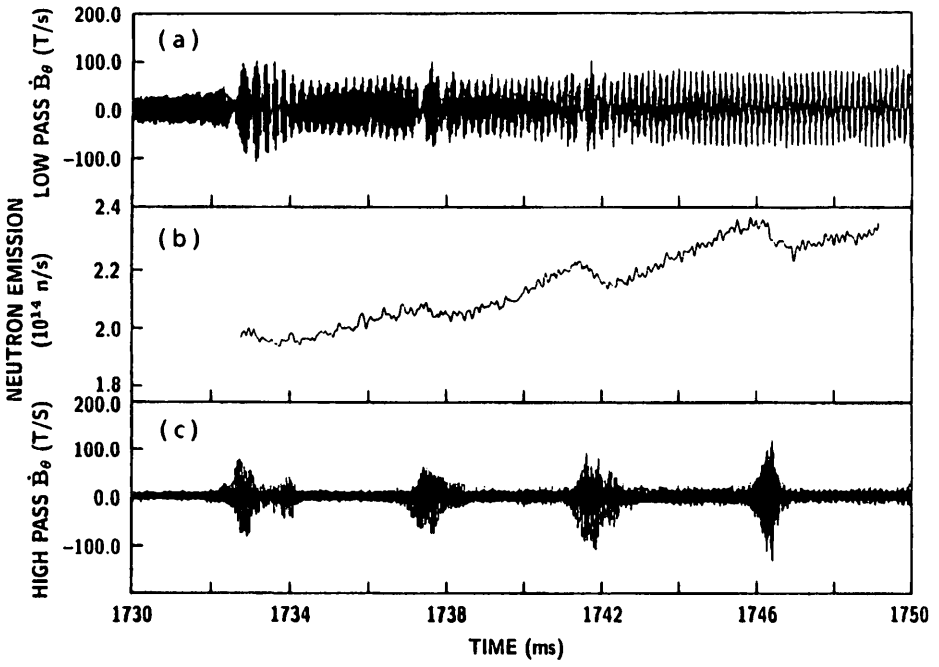

FIG. 2. Signal from a Mirnov coil located near the outer midplane after digital filtering to remove frequencies above 50 kHz (a) and below 100 kHz (c), together with the signal from a plastic scintillator (b). Reductions in neutron emission correlate with high frequency bursts. At 1745 ms, $B_t = 0.8$ T, $I_p = 0.7$ MA, $P_{inj} = 13.1$ MW and $\bar{n}_e = 3.8 \times 10^{13}$ cm^{-3} in a double-null divertor plasma.

Electron temperature and density were measured with multichannel Thomson scattering [29] and by four CO_2 interferometer chords. The effective ion charge Z_{eff} was inferred from Thomson scattering and multichannel visible bremsstrahlung data [30]. A multichannel visible spectrometer system was tuned to measure the helium charge exchange recombination line at 468.6 nm for T_i measurements or H_α light for beam deposition measurements [31]; T_i was also determined from the neutron emission during $H^0 \rightarrow D^+$ injection. In the $H^0 \rightarrow D^+$ experiments, the ratio of hydrogen density to deuterium density was measured at the edge spectroscopically, using the ratio of H_α light to D_α light, and the central deuterium concentration n_d/n_e was inferred from the neutron emission at the end of a 2 ms deuterium beam pulse [32].

3. EXPERIMENT

3.1. Instability data

In $D^0 \rightarrow D^+$ plasmas with large beam and plasma betas and relatively low Alfvén velocity, instabilities that may be related to TAE modes were observed. The conditions for instability are summarized in Section 3.2; here, we describe the instabilities. Figure 2 shows time traces from a magnetic probe near the outboard midplane and from a neutron scintillator. The magnetic probe trace has been digitally filtered to reveal a pair of semi-continuous, low frequency modes (Fig. 2(a)) and bursts of high frequency oscillations (Fig. 2(c)). Each high frequency burst correlates with a sudden reduction in 2.5 MeV neutron emission (Fig. 2(b)). These sudden reductions in neutron signal are an indication that beam ions are lost from the plasma centre at the bursts [19]. The magnitude (~6%) and repetition rate (~220 Hz) of the neutron drops imply a beam ion confinement time [19] of approximately 75 ms. Since the thermalization time ν_E^{-1} was approximately 60 ms in this discharge, this implies [33] that a substantial fraction (~45%) of the beam power is lost owing to these bursts.

These oscillations generally do not appear as a pure mode in the Fourier spectrum (Fig. 3(a)). Figure 3(a) shows the cross-power spectrum of the $\dot{B}_\theta$ signals from two magnetic probes that are spaced 45° toroidally during the burst at 1746 ms shown in Fig. 2. The toroidal mode numbers associated with the various spectral peaks have been obtained from a separate analysis using seven probes with toroidal spacings down to 6° (Fig. 4). The semi-continuous low

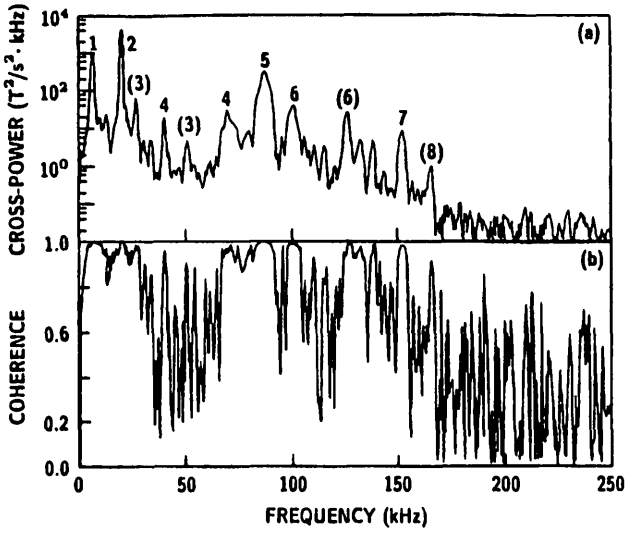

FIG. 3. Spectra of cross-power (a) and coherence (b) of two $\dot{B}_\theta$ signals between 1745.4 ms and 1747.4 ms in the discharge shown in Fig. 2. The coils are at the same poloidal location on the outer wall, displaced 45° from one another. The peaks are labelled with their toroidal mode number; parentheses indicate that the identification is somewhat uncertain.

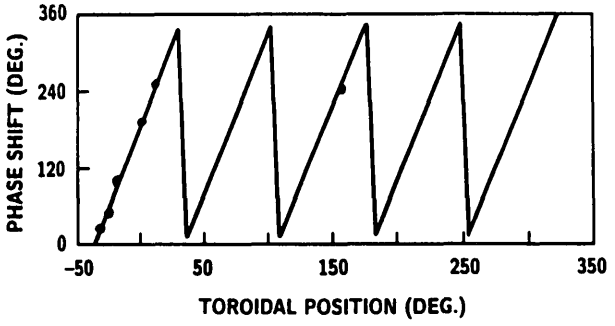

FIG. 4. Phase shift versus toroidal angle for the 87 kHz peak shown in Fig. 3(a). The fit indicates a toroidal mode number $n = 5$.

frequency modes are a 7 kHz/n = 1 mode and a 20 kHz/n = 2 mode. Several peaks at 50–200 kHz are associated with the high frequency bursts. The good coherence of these oscillations between widely spaced probes is shown in Fig. 3(b). The most prominent of the high frequency peaks are those at 70–101 kHz, having consecutive toroidal mode numbers n = 4–6. These oscillations have a non-zero velocity of propagation relative to the bulk plasma. This is readily seen from Fig. 3(a), where the toroidal rotation frequency f_{lab}/n of the n = 5 mode is about 17 kHz. In contrast, the toroidal rotation frequency of the n = 2 mode is only about 10 kHz, which is comparable to the toroidal rotation frequency of the bulk plasma (measured with the charge exchange recombination diagnostic on a similar discharge).

These high frequency oscillations are also observed by other fluctuation diagnostics. SXR measurements from a different discharge indicate that high frequency bursts can locally flatten the SXR emission profile (Fig. 5).

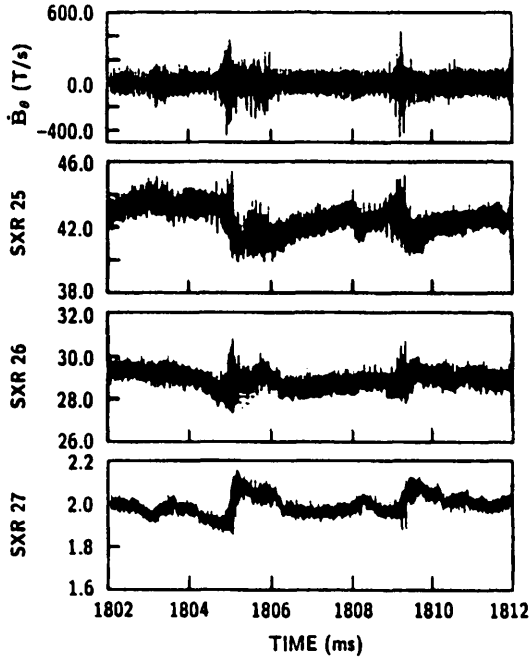

FIG. 5. Signals from a Mirnov coil and from three SXR channels for the discharge shown in Fig. 10. The minimum radius for the three SXR sightlines is at $\rho/\rho_{sep} = 0.47, 0.53$ and 0.61, respectively, where ρ is the toroidal flux co-ordinate and ρ_{sep} is the toroidal flux enclosed within the separatrix. High frequency bursts that cause a local flattening of the SXR profile occur at 1805 ms and 1809.5 ms.

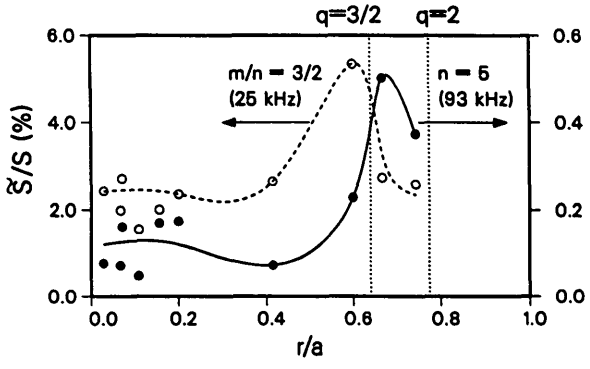

FIG. 6. SXR fluctuation amplitude $\tilde{S}$ normalized to the average amplitude S as a function of ρ/ρ_{sep} for a 25 kHz, m/n = 3/2 mode and a 93 kHZ, n = 5 mode in a double-null divertor discharge with $B_T = 1.0$ T, $I_p = 0.9$ MA, $P_{inj} = 15.6$ MW and $\bar{n}_e = 4.4 \times 10^{13}$ cm^{-3}. The location of the q = 3/2 and q = 2 surfaces (calculated by EFIT [34]) are also shown. The radial structure of the 93 kHz mode is consistent with an n = 5, m = 7–8, TAE mode.

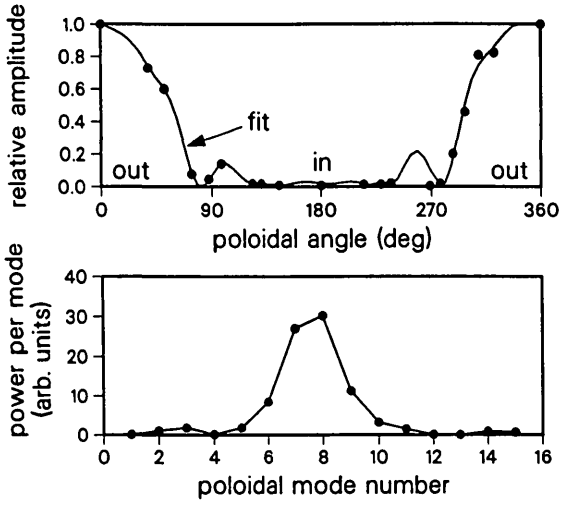

FIG. 7. Cross-power of the $\dot{B}_\theta$ oscillation from a poloidal array of Mirnov coils for the 93 kHz mode shown in Fig. 6. The reference signal is located near the outer midplane (near 0°). Analysis of the signals indicates that the m = 7 and m = 8 poloidal harmonics predominate, as expected for an n = 5 TAE mode located near the q = 1.5 surface.

Spectral analysis indicates that these bursts consist of a cluster of peaks at 57, 78, 93, 108 and 123 kHz, with successively increasing toroidal mode numbers n = 3–7. Although the magnitude of the change in the SXR signals is not large, it demonstrates that the high frequency modes can have an observable effect on the thermal plasma. The radial structure of the instability is obtained from SXR measurements. In Fig. 6, the fluctuation amplitude of a low frequency mode and of a high frequency mode is plotted as a function of position. Also shown are the radial locations of the q = 1.5 and q = 2 surfaces computed from an MHD equilibrium fit [34] based on kinetic profile and magnetics data. The high frequency mode peaks just outside the calculated q = 1.5 surface (Fig. 6).

Measurements with magnetic probes at the vacuum vessel wall indicate that the oscillation amplitude is strongly localized on the large major radius side. Figure 7 shows the cross-power of a poloidal array of $\dot{B}_\theta$ signals for the n = 5, 93 kHz mode shown in Fig. 5. The large amplitude variation in the poloidal direction implies that a mixture of several poloidal modes must be present. However, the non-circular cross-section of DIII-D makes it difficult to find a suitable poloidal co-ordinate in which to decompose the mode structure. A simple decomposition has been performed using

$$\tilde{B}(\omega) = \Sigma B_m(\omega) \exp(im\theta) \qquad (3)$$

where $\tilde{B}(\omega)$ is the complex Fourier amplitude and θ is the poloidal angle relative to the centre of the vacuum vessel (corrected for an elongation $\kappa = 1.5$ at $q \simeq 1.5$). The analysis indicates that the mode amplitude is largest for m = 7 and m = 8 (Fig. 7), as expected for an n = 5 mode situated near the q = 1.5 surface.

To compare the measured frequency with theory (which is calculated in a stationary frame), it is necessary to correct for the Doppler shift introduced by bulk plasma rotation. Since the plasma rotation frequency is typically 10–18 kHz, this correction is substantial for moderate n modes. Unfortunately, the measurements of plasma rotation are only accurate to approximately 20%, which introduces an unacceptably large uncertainty in the inferred frequency. For a more accurate determination of the frequency in the plasma frame f, we measure the frequency shift Δf between modes in a 'cluster' of high frequency peaks (for example, $\Delta f \simeq 17$ kHz for the three peaks near 100 kHz in Fig. 3(a)). We then *assume* that the separation between the peaks is due primarily to the Doppler shift and use the measured spacing between peaks Δf to obtain the mode frequency in the plasma frame, $f = f_{lab} - n\Delta f$. The validity of this assumption was checked by plotting the radial profile of the SXR emission (as in Fig. 6) for all of the modes in a few representative spectra. It was found that the spatial profile of $\tilde{S}/S$ was similar for all the

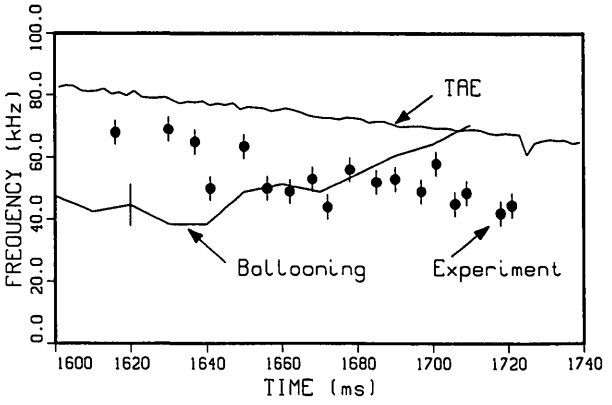

FIG. 8. Time evolution of the frequency of an n = 6 high frequency mode in the discharge of Fig. 2. The frequency is determined from fast Fourier transforms of Mirnov signals over 2 ms intervals. A correction for the Doppler shift is included. The curve labelled TAE is the nominal prediction for a gap mode at the q = 1.5 surface, with the toroidal field and major radius evaluated at the magnetic axis. An increase in density of ~50% is responsible for the drop in f_{TAE}. The curve labelled ballooning is evaluated from measurements of the ion temperature profile using Eq. (4); the vertical line indicates the typical random error associated with the spline fit. An increase in T_i of ~80% is responsible for the increase in ω_{*i}.

modes in a cluster of peaks. Thus, if one further assumes that modes localized near the same rational surface have the same propagation velocity (as expected for TAE modes), the frequency in the plasma frame can be deduced from the measured frequencies f_{lab} and Δf alone.

In Fig. 8, the time evolution of the Doppler corrected frequency f of an n = 6, ~150 kHz peak is compared with TAE theory for the discharge of Fig. 2. In this case, neutral beam sources were steadily added to the discharge, causing the electron density to increase steadily from 2.2×10^{13} cm^{-3} at 1600 ms to 3.4×10^{13} cm^{-3} at 1720 ms. During this period, the beam power injected by the more tangential ('left') sources increased from 4.5 MW to 6.7 MW, the total plasma beta increased from 3.4% to 5.6%, and the central ion temperature increased from 2.2 kV to 4.0 kV. Throughout this time, a cluster of evenly spaced peaks appeared in the Mirnov power spectrum. (After a minor disruption at 1723 ms, the spectrum changed character, and it is no longer possible to identify with confidence the same cluster of peaks.) Theoretically [10], the frequency of a TAE mode is approximately $f_{TAE} \simeq v_A/4\pi qR$. Since the toroidal field (0.8 T) and the plasma current (0.7 MA) were constant during this time period, f_{TAE} decreases in time owing to the increasing plasma density (Fig. 8). The measured mode frequency exhibits a similar trend (Fig. 8). However, the magnitude of the observed frequency is smaller than the predicted frequency by about 30%. In the theoretical prediction, $q \simeq 1.5$ (based on SXR measurements in other discharges), R = 167 cm and B(R = 167 cm) = 0.8 T were assumed. If R = 200 cm is employed, as suggested by the poloidal structure of the mode (Fig. 7), then the theoretical prediction is reduced by 30%, in agreement with experiment. Other possible explanations for the difference between f and f_{TAE} are discussed in Section 4.

Since the high frequency modes are observed in high beta plasmas ($\beta_n \gtrsim 2.5$), one possibility is that they are ballooning modes rather than TAE modes. Chen [11] has shown that low frequency ballooning modes with $n \lesssim 10$ can be destabilized by circulating fast ions. The predicted frequency for these kinetically destabilized ballooning modes is $\omega \simeq \omega_{*i}$ [11], where ω_{*i} is the ion diamagnetic frequency. The diamagnetic frequency at the q = 1.5 surface can be estimated from the ion temperature profiles measured by the charge exchange recombination diagnostic [31] using the formula

$$\frac{\omega_{*i}}{2\pi} = \frac{k_\theta}{2\pi}\frac{c}{n_i e_i B}\frac{dp_i}{dr}$$

$$\simeq \frac{m}{2\pi\sqrt{ab}}\frac{c}{e_i B}\frac{\Delta T_i}{\Delta R} \qquad (4)$$

In Eq. (4), the poloidal wave number is assumed to be that of an m = 9 mode (m = qn) at the average

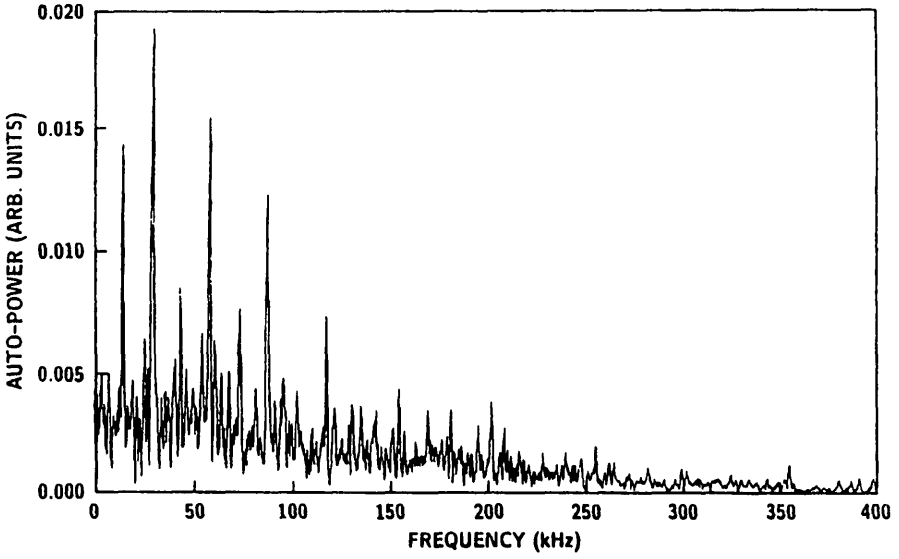

FIG. 9. Auto-power spectrum of a reflectometer channel with a cut-off layer of $\bar{n}_e = 1.3 \times 10^{13}$ cm^{-3} between 1807 ms and 1812 ms for the discharge shown in Fig. 5. The high frequency peaks at 57, 93 and 123 kHz coincide (within 2 kHz) with peaks observed with the Mirnov coils.

minor radius of the q = 1.5 surface, and the pressure gradient is assumed to equal the temperature gradient alone ($(dp_i/dr) \simeq n_i(dT_i/dr)$). The latter assumption is justified by the very flat electron density profile measured by Thomson scattering (the ion density profile is not measured in DIII-D). The temperature gradient is inferred from a spline fit to the measured eight-point profile; if the profile is not smooth, the inferred gradient is erroneous. In Fig. 8, the time evolution of $\omega_{*i}/2\pi$ is compared with the time evolution of the mode frequency f. Although the magnitude of ω_{*i} is in reasonable agreement with experiment, the time evolution is not. The mode frequency f decreases by ~30% between 1600 ms and 1720 ms, while ω_{*i} *increases* by ~60%. This suggests that the observed instability is probably not a low frequency ballooning mode.

The SXR data (and the neutron data) demonstrate that the high frequency modes are not localized in the plasma edge. The modes are often coupled to edge modes, however. Figure 9 shows the auto-power spectrum of a reflectometer signal at one of the bursts shown in Fig. 5. This channel measures density fluctuations from the cut-off layer near 1.3×10^{13} cm^{-3}, which is at the plasma edge in this discharge. Some of the high frequency oscillations observed with the Mirnov coils (57 kHz and 93 kHz peaks) are evident in the spectrum.

High frequency bursts have not been observed by the FIR scattering diagnostic [26]. This is expected, since the wave number of modes with $m \lesssim 10$ is smaller than the instrumental resolution of <2.5 cm^{-1}.

The trends described above are representative of all the available data. In discharges with fishbone bursts [35], high frequency bursts sometimes occur at the fishbone bursts and sometimes during the quiescent period between fishbones. Bursts also are observed during semi-continuous low n MHD activity (as in Figs 2 and 5). When bursts are observed, the spectrum always exhibits at least one set of fairly evenly spaced peaks with increasing toroidal mode numbers. Frequencies of up to 210 kHz and mode numbers between n = 2 and n = 10 have been observed. The frequency spacing Δf between high frequency peaks in the spectrum often coincides with the frequency of a fishbone or other low frequency mode. This suggests that the cluster of peaks could actually be a single unstable mode that is modulated in amplitude by the low frequency mode [22]. This amplitude modulation, caused by the periodic variation in plasmas conditions related to the low frequency mode, may occur in the actual instability in the plasma or only in the signal which reaches the probe. Alternatively, the presence of the low frequency mode may couple a single unstable high frequency mode to neighbouring modes that would otherwise be stable. On the other hand, in some cases, the spacing between high frequency peaks Δf differs by 4–5 kHz from the frequency of the n = 1, low frequency mode and, in a few cases, the successive peaks are irregularly spaced in frequency. These cases also support the hypothesis that each peak coincides with an unstable mode.

For the cases analysed, the radial profile generally peaks at a location different from that of the low n modes and has a spatial width (FWHM) of order 10 cm. The poloidal variation in mode amplitude is always large and can exceed the in-out variation in low-n amplitude by a factor of ten. There is usually evidence of coupling to edge fluctuations. The inferred mode frequency is usually smaller than the nominal value $f_{TAE} = v_A/4\pi qR$ evaluated at q = 1.5 and R = 167 cm ($f \simeq 0.2$–$0.8 f_{TAE}$). There is no evident correlation between the inferred mode frequency and the Alfvén velocity for different discharge conditions, although any dependence could be obscured by differing values of q. The ratio f/f_{TAE} also does not appear to depend

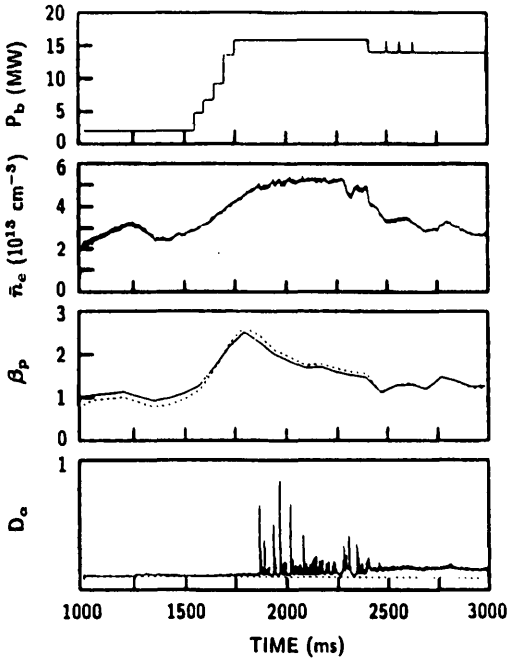

FIG. 10. Time evolution of the beam power, the line averaged electron density, the poloidal beta (measured by equilibrium coils (solid) and a diamagnetic loop (dotted)), and the D_α light from the outer divertor strike point in the $D^0 - D^+$ discharge shown in Figs 5 and 9. The spikes in the D_α emission are giant ELMs. At 1830 ms, $B_t = 1.0$ T, $I_p = 0.7$ MA, $P_{inj} = 15.8$ MW, $\bar{n}_e = 5.0 \times 10^{13}$ cm^{-3}, $Z_{eff} \simeq 3.5$, $T_e(0) \simeq 2.1$ kV and $T_i(0) \simeq 3.3$ kV.

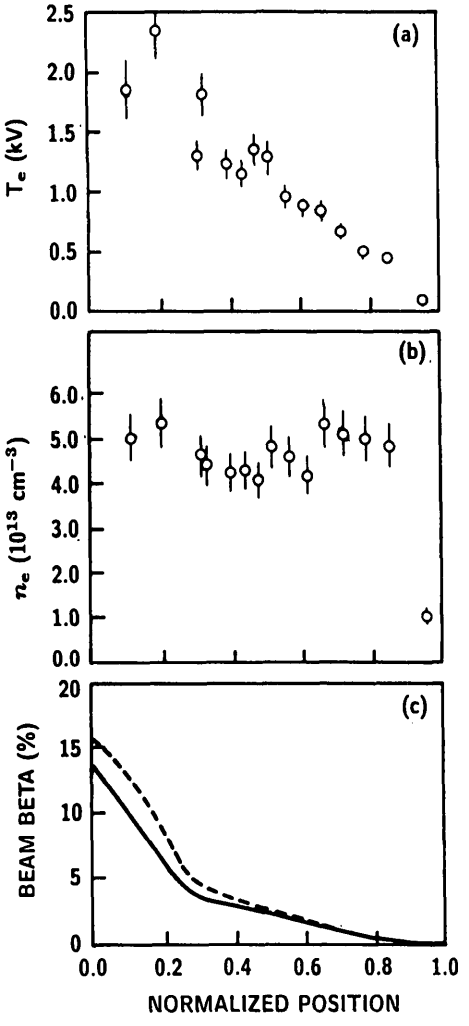

FIG. 11. (a) Profile of electron temperature versus position at 1830 ms for the $D^0 \rightarrow D^+$ discharge shown in Fig. 10. The vertical Thomson scattering data have been mapped onto toroidal flux co-ordinates using a flux surface reconstruction based on magnetics measurements [34]. (b) Profile of electron density versus ρ/ρ_{sep}. The Thomson scattering data have been renormalized to agree with the interferometer measurements. (c) Beta of full energy beam ions calculated by MCGO [36] versus ρ/ρ_{sep}. The solid line is the parallel beta of the full energy ions and the dotted line is the total beta β_f^{full}. Because this discharge was unstable, the actual distribution may differ from the distribution calculated by MCGO.

on the normalized beta. The Doppler shift correction is always large in our set of data (typically, $f \sim \frac{1}{3} f_{lab}$), so errors in this correction may also obscure the actual dependences.

3.2. Conditions for instability

The principal data for this study were obtained in several days of $D^0 \rightarrow D^+$ experiments that had the goal

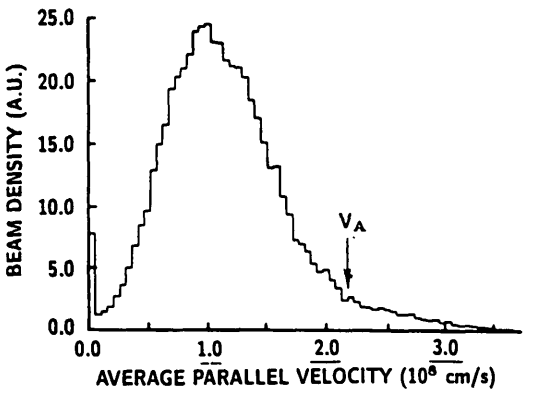

FIG. 12. (a) Number of beam ions as a function of circulation velocity at 1830 ms in the discharge of Fig. 10. The ions near the origin are trapped. The Alfvén velocity is indicated (since the density profile was very flat in this H-mode discharge, the Alfvén velocity profile was virtually constant). Because this discharge was unstable, the actual distribution may differ from the distribution calculated by MCGO [36].

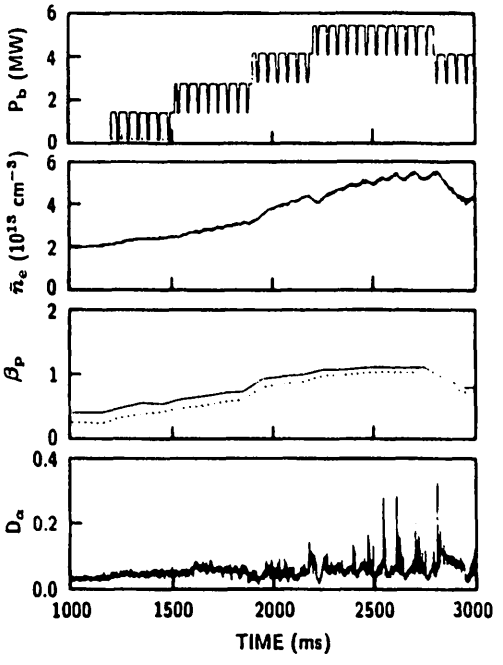

FIG. 13. Time evolution of the beam power, the line average electron density, the poloidal beta and the D_α light in an $H^0 \rightarrow D^+$ discharge. The 150° tangential beam was intentionally modulated for active charge exchange measurements. At 2500 ms, $I_p = 0.7$ MA, $B_t = 0.73$ T, $P_{inj} = 5.6$ MW, $\bar{n}_e = 4.5 \times 10^{13}$ cm^{-3} and $Z_{eff} \simeq 2.5$.

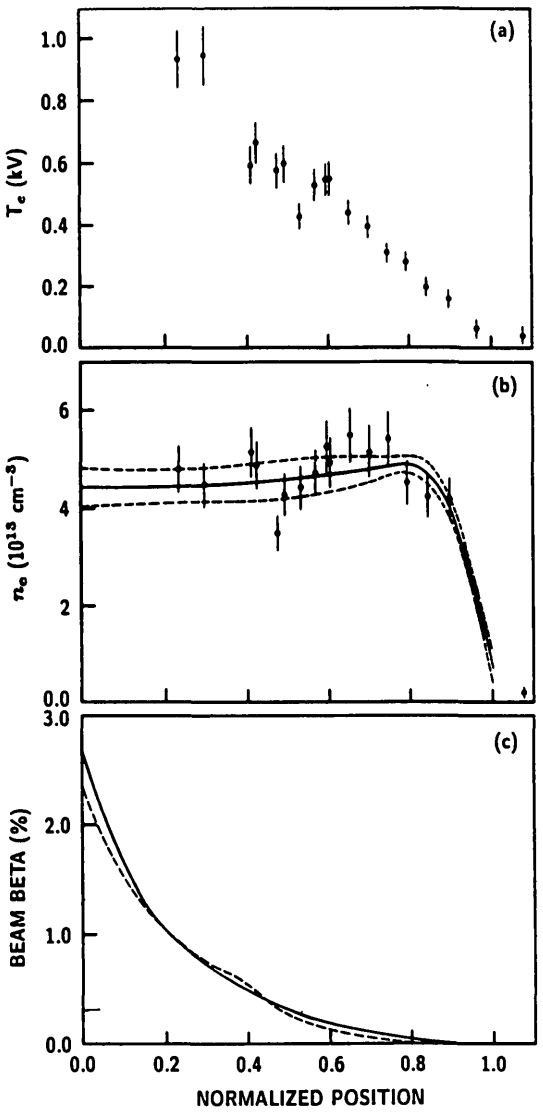

FIG. 14. (a) Profile of the electron temperature measured by Thomson scattering versus ρ/ρ_{sep} at 2500 ms for the $H^0 \rightarrow D^+$ discharge shown in Fig. 13. (b) Profile of the electron density versus ρ/ρ_{sep}. The points are from Thomson scattering and the fit includes interferometer data. (c) Beta of full energy beam ions calculated by MCGO [36] versus ρ/ρ_{sep}.

of maximizing the normalized beta and in two days of $H^0 \rightarrow D^+$ experiments devoted to investigating the regime $v_{\|0}/v_A > 1$. Most of the discharges studied here were double-null divertor H-mode discharges, although a few L-mode discharges were studied during the dedicated $H^0 \rightarrow D^+$ experiments.

Figure 10 shows the time evolution of the neutral beam power, the electron density, the poloidal beta and a divertor D_α signal in the $D^0 \rightarrow D^+$ discharge shown in Fig. 5. High frequency bursts were observed in this discharge during the period of intense beam injection before 1835 ms, when the beta saturated. The central electron temperature measured by Thomson scattering was ~2 kV (Fig. 11(a)) and the density profile was relatively flat (Fig. 11(b)), which implies that the Alfvén velocity was approximately 2.2×10^8 cm/s and roughly constant across the plasma. Monte Carlo calculations [36] of beam deposition and Coulomb scattering indicate that the pressure from full energy beam ions peaked strongly on axis for these discharge conditions (Fig. 11(c)). The calculated volume average beam beta of full energy ions was $\langle\beta_f\rangle = 1.8\%$, with the perpendicular pressure exceeding the parallel pressure by ~18%. On axis, the calculations give $\beta_f^{full} \simeq 15\%$, but reductions in neutron emission at high frequency bursts were observed on this discharge, so the actual pressure was probably smaller. Figure 12 shows the calculated distribution of circulation frequencies for the total beam ion population (averaged over the plasma volume). The nominal parallel velocity of full energy tangentially injected beam ions that ionize on axis is $v_{\|0} = 1.8 \times 10^8$ cm/s, which is less than the Alfvén velocity for this condition; however, because of substantial pitch angle scattering in this warm, high Z_{eff} plasma, some of the full energy beam ions are calculated to be super-Alfvénic (Fig. 12).

Figure 13 shows one of the more interesting plasmas from an $H^0 \rightarrow D^+$ day. The basic idea of the experiment was to stack tangential beams progressively until evidence of instability appeared in the charge exchange and fluctuation data. The central electron temperature measured by Thomson scattering (Fig. 14(a)) was approximately 1.0 kV; the neutron emission also gave $T_i(0) \simeq 1.0$ kV. The electron density profile was rela-

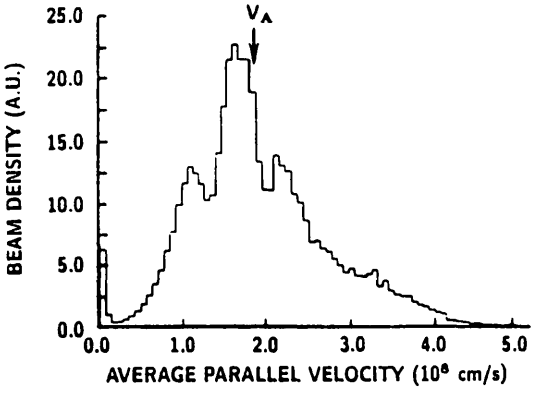

FIG. 15. Number of beam ions as a function of circulation velocity at 2500 ms for the discharge of Fig. 13. The Alfvén velocity is indicated (since the density profile was very flat in this H-mode discharge, the Alfvén velocity profile was virtually constant).

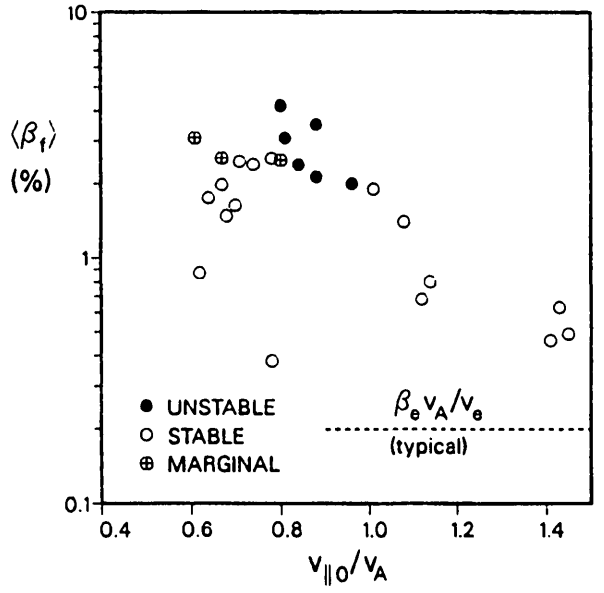

FIG. 16. Discharge conditions studied in $\langle\beta_f\rangle$ and $v_{\|0}/v_A$ space. The ordinate is the volume averaged beam beta (computed by MCGO [36] for several cases and estimated from the beam power, the central deceleration rate and the toroidal field for the other cases). Most points represent several similar discharges. The unstable discharges exhibited high frequency activity similar to that described in Section 3.1. B_t = 0.7-1.5 T, $\bar{n}_e$ = (2.8-6.3) × 10^{13} cm^{-3}, P_{inj} = 4.2-18.4 MW. The actual beam beta may be smaller than the calculated value because of losses associated with instabilities. The nominal threshold in beam beta predicted by Eq. (1) is indicated.

tively flat (Fig. 14(b)) and the hydrogen concentration was ~1/3, which implies that the Alfvén velocity was approximately 1.8 × 10^8 cm/s and roughly constant across the plasma. The pressure from full energy beam ions peaked strongly on axis (Fig. 14(c)). Figure 15 shows the distribution of the circulation velocity for the beam ion population; most of the ions injected at full energy have $v_\| > v_A$.

The different conditions studied are summarized in Fig. 16. For the plasma parameters studied, $\bar{n}_e$ varied between 2.2 × 10^{13} cm^{-3} and 6.3 × 10^{13} cm^{-3}, B_t varied between 0.7 T and 1.5 T, and the beam power varied between 4.2 MW and 18.4 MW. High frequency fluctuations (Section 3.1) were only observed for $v_{\|0}/v_A \geq 0.8$ and $\langle\beta_f\rangle \geq 2.0\%$ (Fig. 16) in high β_n discharges ($\beta_n \geq 3.2$). Discharges with very high beam beta and plasma beta ($\beta_n \geq 3.6$) have been obtained at 1.2 T (data point for $\langle\beta_f\rangle = 3.0\%$ and $v_{\|0}/v_A = 0.61$ in Fig. 16), but the amplitude of high frequency activity was two orders of magnitude smaller than that in discharges with $v_{\|0}/v_A \geq 0.8$. Detectable fluctuations were absent in all of the $H^0 \rightarrow D^+$ discharges (data points for $v_{\|0}/v_A > 1.1$ in Fig. 16). Although $v_\|/v_A$ exceeded one and $\langle\beta_f\rangle$ as large as 1.4% was obtained, no evidence of Alfvén instabilities was observed.

In addition to the fluctuation data, active charge exchange data were examined for evidence of anomalous beam ion behaviour in the $H^0 \rightarrow D^+$ discharges. The active charge exchange signal Φ (after corrections for neutral attenuation) divided by the tangential beam power $P_\|$ was compared with estimates of $(\beta_f/\beta_e)(v_e/v_A)$, which is related to the theoretical growth rate for TAE instability (Eq. (1)). One might have expected a reduction in $\Phi/P_\|$ as the beam beta increased, but no correlation of $\Phi/P_\|$ with $(\beta_f/\beta_e)(v_e/v_A)$ was observed. This is consistent with the fact that no high frequency instabilities were observed in these discharges.

4. DISCUSSION

Theoretically, four conditions must be satisfied for TAE instability [10, 12]: a gap must exist in the Alfvén spectrum, the fast ions must be nearly super-Alfvénic, the fast ion gradient must be peaked ($\omega_{*f} \geq \frac{1}{2}\omega$) and the fast ion beta must be large enough to overcome electron damping. Calculations using Eq. (8) of Ref. [10] indicate that a gap does exist for an n = 4 mode in a circular plasma for DIII-D q and v_A profiles. The beam ions are super-Alfvénic in some DIII-D plasmas (Figs 12 and 15). The condition $\omega_{*f} \geq \frac{1}{2}\omega$ is satisfied in DIII-D, since, even for m = 1, $\omega_{*f} \simeq \frac{1}{2}\omega$. (Here, and in the evaluation of F in Table II, we follow Fu and Van Dam [10] and evaluate ω_{*f} at $E_{inj}/3.5$.) According to the approximate expression derived by Fu and Van Dam (Eq. (1)), the local beam beta must exceed $\beta_e(v_A/v_e)/[F(\omega_{*f}/\omega - \frac{1}{2})]$ for instability. Assuming F = O(1), this implies $\beta_f/\beta_e \geq 2\%$ for instability, which is easily satisfied for $\bar{n}_e \leq 5 \times 10^{13}$ cm^{-3} in DIII-D. Thus, all the discharges with $v_\|/v_A \geq 1$ in Fig. 16 satisfied Fu and Van Dam's approximate criteria for instability. (Chen's approximate criterion for β_f [11] was also met.) Using the plasma parameters of Figs 10–15 to evaluate the quantities in Eq. (1), the ratio of the beam drive term to the electron damping term was more than ten in both the unstable $D^0 \rightarrow D^+$ plasmas and the stable $H^0 \rightarrow D^+$ plasmas (Table II). Thus, it appears that the experimental threshold for instability is one order of magnitude larger than that given in Eq. (1). It is not possible to exclude entirely the possibility that small amplitude TAE modes exist for $\langle\beta_f\rangle < 1\%$, but, if they do, their amplitude is at least two orders of magnitude smaller than the modes observed when $\langle\beta_f\rangle \geq 2\%$. A more likely possibility is that electron damping at the edge of the gaps, which is neglected in the approximate theories [10, 11], accounts for the higher threshold.

TABLE II. THE TAE INSTABILITY CRITERION (Eq. (1)) IN DIII-D

Plasma	$D^0 - D^+$ (Figs 10–12)	$H^0 - D^+$ (Figs 13–15)
v_A (cm/s)	2.2×10^8	1.8×10^8
ω (rad/s) [a]	4.4×10^5	3.6×10^5
$v_{\|0}/v_A$	0.82	1.4
F [b]	0.82	2.4
Beam scale length (cm) [c]	40	40
ω_{*f}/m (rad/s) [d]	1.3×10^5	1.3×10^5
β_f [e]	2.5%	0.3%
β_e [f]	2.4%	1.3%
v_e (cm/s)	2.3×10^9	1.9×10^9
Local damping [g]	2.3×10^{-3}	1.3×10^{-3}
m	7	7 [h]
Drive/damping [i]	14	11

[a] Theoretical $v_A/2qR$, using q = 1.5 and R = 167 cm.
[b] Using the expression of Fu and Van Dam, with $v_\alpha = v_{\|0}/\sqrt{3.5}$.
[c] $(d \ln n_f/dr)^{-1}$ at the q ≃ 1.5 surface.
[d] $c(E_{inj}/3.5)(d \ln n_f/dr)/(\sqrt{a}beB)$.
[e] Of the full-energy component at the q ≃ 1.5 surface.
[f] At the q ≃ 1.5 surface.
[g] $\beta_e v_A/v_e$.
[h] Assumed.
[i] $[\beta_f(\omega_{*f}/\omega - \frac{1}{2})F]/[\beta_e v_A/v_e]$.

The theoretical assumptions that $\beta_f \ll \beta$, that the aspect ratio is large, that the plasma shape is circular, and that the distribution function is Maxwellian are also invalid for DIII-D conditions. It is also possible that collisional damping is important since $\nu_{ei} \sim 0.1\omega$. Finally, the observation of similar fluctuations in the plasma edge (Fig. 9) suggests a coupling to edge modes, which would be heavily damped and would provide additional stabilization.

The observed fluctuations (Fig. 3) are probably TAE modes. The fluctuations do not appear to be driven by plasma pressure alone, since similar discharges with $\beta_n \simeq 3.6$ but $v_{\|0}/v_A = 0.6$ are marginally stable (Fig. 16). The fluctuations are only observed when all the conditions for TAE instability are satisfied. The spatial structure (Fig. 6) and the fact that two adjacent m numbers dominate the poloidal structure also suggest identification as TAE modes. The frequency is more problematic, however. The comparison between theory and experiment is complicated by uncertainties in q and R and by large Doppler shift corrections. Within a single discharge, the dependence of frequency on density is consistent with theoretical expectations (Fig. 8). However, in many cases, such as the one documented in Figs 10–12, the frequency in the plasma frame is only ~1/3 of the theoretical prediction. One possibility is that finite plasma pressure is responsible for the reduced frequency. Fu and Cheng [37] found that the frequency of a high n gap mode drops into the continuum as the pressure gradient reaches the ballooning limit. The width of the gap $\omega_0 - \omega_-$ depends on toroidicity roughly as $r_0/R + \Delta'$, where r_0/R is the inverse aspect ratio and Δ' is the radial derivative of the Shafranov shift [12]. Owing to the small aspect ratio and the large Shafranov shift of the DIII-D plasmas, the continuum gap is rather large in DIII-D, so this effect could result in a ~40% downshift in frequency. A similar result was found by Spong et al. [38], who computed a factor of three reduction in the real frequency for high-n TAE modes near the ballooning limit. Thus, the discrepancy in frequency between theory and experiment may be associated with the high beta of the thermal plasma.

Phenomenologically, the modes appear to be similar to the high frequency bursts observed on PDX [19] and PBX [20]. The magnitude of the drop in neutron emission at high frequency bursts with $\tilde{B}_\theta/B_\theta \sim 10^{-3}$ (Fig. 2) is comparable to the observations in PBX [39]. Another similarity is that the PDX, PBX and DIII-D modes all occurred in plasmas with large β_n and β_f. Weiland and Chen [40] suggested that the PDX instability is a trapped particle driven ballooning mode, and Biglari and Chen [41] extended this analysis to include resistivity. This identification seems unlikely in DIII-D, however, since few trapped particles are expected (Fig. 12) and since the stability of the mode appears to depend upon $v_\|/v_A$ (Fig. 16). The high frequency bursts in PBX [20] occurred when $v_\|/v_A \simeq 0.64$. Chen suggested that the bursts in PBX were low frequency ballooning modes with frequency $\omega \simeq \omega_{*i}$, where ω_{*i} is the ion diamagnetic frequency [11]. Although this is a possible explanation for the modes observed in DIII-D, the time evolution of ω_{*i} in the discharge of Fig. 8 seems inconsistent with the experimental behaviour.

There is no evidence of spatially extended, low n, propagating modes similar to GAE modes in DIII-D plasmas. Campbell [42] predicted GAE instability for a DIII-D discharge, but his calculations neglected toroidal effects, which have been shown to be strongly stabilizing [7, 8]. Since the drive term, which is proportional to the gradient of the Alfvén velocity, is virtually zero over most of the volume in these H-mode plasmas, it is not surprising that no such modes are observed.

The rapidly rising q profile associated with a separatrix may also provide additional stability.

Anomalous fast ion behaviour has been observed with charge exchange diagnostics during intense $H^0 \rightarrow D^+$ beam injection into ISX-B [43], in $D^0 \rightarrow D^+$ experiments in TFR [44], during fishbone instability in PDX [45], and in high beta plasmas in Doublet III [16]. For our $H^0 \rightarrow D^+$ conditions, however, any anomalous behaviour is below our level of detectability.

5. CONCLUSION

Instabilities with most of the expected features of TAE modes are observed in DIII-D. The modes are observed only in the presence of a large, fast ion population that is nearly super-Alfvénic. They propagate in the plasma frame, transport fast ions and are spatially localized near a spectral gap, as expected for TAE modes. The mode frequency is lower than predicted for TAE modes, but the reduction in frequency may be related to the large plasma pressure.

The instabilities cause large fast ion losses that could prevent a reactor from igniting. However, the threshold for TAE instability is at least one order of magnitude higher than that predicted by the simple local expressions of Fu and Van Dam [10] and Chen [11]. Instability is only observed when the *volume averaged* fast ion beta exceeds 2% (Fig. 16). If the observed instabilities are not TAE modes, then the threshold for instability is apparently even higher ($\langle\beta_f\rangle \gtrsim 5\%$). Since future devices such as ITER are expected to operate at $\langle\beta_f\rangle \lesssim 1\%$, this suggests the possibility that alphas will not drive TAE modes unstable in a reactor.

Future experimental work will explore possible stabilizing effects associated with H-mode density profiles, plasma shaping and edge shear. An attempt to delineate the role of plasma pressure and of beam ion free energy in the destabilization of the fluctuations will also be made. In addition, we hope to calculate the TAE eigenfunction in realistic DIII-D equilibria for comparison with the poloidal array of Mirnov signals. A full numerical calculation of TAE stability for DIII-D conditions is also desirable. Finally, since it is not possible to drive Alfvén waves without approaching the beta limit, a realistic theory must treat the effect of background plasma pressure on the shear Alfvén branch.

ACKNOWLEDGEMENTS

The support of the DIII-D Operations, Neutral Beam and Physics Groups is gratefully acknowledged, with special thanks to J. Ferron, R. Groebner, D. Hill, T. LeHecka, T. Osborne, C. Petty, R. Pinsker, R. Philipona and R. Seraydarian for their assistance with the measurements. The authors are also grateful to S. Scott of PPPL for giving them the TEXAS charge exchange analysis code and to M. Brown of LLNL and G. Bramson of GA for their assistance in adapting the code for use on DIII-D. Finally, thanks are due to A. Molvik for initiating studies of Alfvén instabilities on DIII-D, and to D. Sigmar, L. Chen and K.-L. Wong for helpful discussions.

This work was supported by the United States Department of Energy under Contract No. DE-AC03-89ER51114.

REFERENCES

[1] TOMABECHI, K., in Plasma Physics and Controlled Nuclear Fusion Research 1988 (Proc. 12th Int. Conf. Nice, 1988), Vol. 3, IAEA, Vienna (1989) 215; POST, D.E., ibid., p. 233.

[2] NISHIDA, A., (Ed.), Magnetospheric Plasma Physics, Center for Academic Publications, Tokyo (1982).

[3] BERK, H.L., HORTON, W., ROSENBLUTH, M.N., RUTHERFORD, P.H., Nucl. Fusion **15** (1975) 819.

[4] MIKHAILOVSKIJ, A.B., Zh. Ehksp. Teor. Fiz. **68** (1975) 1772; Sov. Phys. — JETP **41** (1975) 890; ROSENBLUTH, M.N., RUTHERFORD, P.H., Phys. Rev. Lett. **34** (1975) 1428; TSANG, K.T., SIGMAR, D.J., WHITSON, J.C., Phys. Fluids **24** (1981) 1508.

[5] GOEDBLOED, J.P., Phys. Fluids **18** (1975) 1258.

[6] LI, Y.M., MAHAJAN, S.M., ROSS, D.W., Phys. Fluids **30** (1987) 1466.

[7] CHENG, C.Z., FU, G.Y., Van DAM, J.W., in Theory of Fusion Plasmas (Proc. Joint Varenna-Lausanne Int. Workshop Chexbres, 1988), Editrice Compositori, Bologna (1989) 259.

[8] FU, G.Y., Van DAM, J.W., Phys. Fluids B **1** (1989) 2404.

[9] CHENG, C.Z., CHANCE, M.S., Phys. Fluids **29** (1986) 3695.

[10] FU, G.Y., Van DAM, J.W., Phys. Fluids B **1** (1989) 1949.

[11] CHEN, Liu, in Theory of Fusion Plasmas (Proc. Joint Varenna-Lausanne Int. Workshop Chexbres, 1988), Editrice Compositori, Bologna (1989) 327.

[12] CHENG, C.Z., Alpha Particle Destabilization of the Toroidicity-Induced Alfvén Eigenmodes, Rep. PPPL-2717, Princeton Plasma Physics Laboratory, Princeton, NJ (1990); Phys. Fluids B **3** (1991), in press.

[13] CHENG, C.Z., Fusion Technol. **18** (1990) 443.

[14] SIGMAR, D.J., HSU, C.T., WHITE, R., CHENG, C.Z., Alpha Particle Losses from Toroidicity Induced Alfvén Eigenmodes, Rep. PFC/JA-89-58, Massachusetts Institute of Technology, Cambridge (1989).

[15] LEONOV, V.M., MEREZHKIN, V.G., MUKHOVATOV, V.S., SANNIKOV, V.V., in Plasma Physics and Controlled Nuclear Fusion Research 1980 (Proc. 10th Int. Conf. Brussels, 1980), Vol. 1, IAEA, Vienna (1981) 393.

[16] ARMENTROUT, C.J., STRAIT, E.J., Evidence For Prompt Fast Ion Loss From Plasmas During Neutral Beam Injection in Doublet III, Rep. GA-A 17891, General Atomics, San Diego, CA (1986).
[17] MURAKAMI, M., SWAIN, D.W., BATES, S.C., et al., in Plasma Physics and Controlled Nuclear Fusion Research 1980 (Proc. 10th Int. Conf. Brussels, 1980), Vol. 1, IAEA, Vienna (1981) 377; DUNLOP, J.L., CARRERAS, B.A., PARÉ, V.K., et al., Phys. Rev. Lett. **48** (1982) 538.
[18] YAMAMOTO, S., MAENO, M., SUZUKI, N., et al., Nucl. Fusion **21** (1981) 933.
[19] STRACHAN, J.D., GREK, B., HEIDBRINK, W., et al., Nucl. Fusion **25** (1985) 863.
[20] HEIDBRINK, W.W., BOL, K., BUCHENAUER, D., et al., Phys. Rev. Lett. **57** (1986) 835.
[21] WONG, K.-L., FONCK, R.J., PAUL, S.F., et al., Phys. Rev. Lett. **66** (1991) 1874.
[22] STRAIT, E.J., Bull. Am. Phys. Soc. **34** (1989) 1939.
[23] LUXON, J.L., DAVIS, L.G., Fusion Technol. **8** (1985) 441.
[24] SNIDER, R.T., EVANKO, R., HASKOVEC, J., Rev. Sci. Instrum. **59** (1988) 1807.
[25] LEHECKA, T., PEEBLES, W.A., LUHMANN, N.C., Jr., BURNS, S.R., OLSON, E., DIII-D Group, Rev. Sci. Instrum. **59** (1988) 1620.
[26] PHILIPONA, R., DOYLE, E.J., LUHMANN, N.C., Jr., et al., Rev. Sci. Instrum. **61** (1990) 3007.
[27] HEIDBRINK, W.W., Rev. Sci. Instrum. **57** (1986) 1769.
[28] HEIDBRINK, W.W., Rev. Sci. Instrum. **59** (1988) 1679.
[29] HSIEH, C.L., CHASE, R., DeBOO, J.C., et al., Rev. Sci. Instrum. **59** (1988) 1467.
[30] SCHISSEL, D.P., STOCKDALE, R.E., St. JOHN, H., TANG, W.M., Phys. Fluids **31** (1988) 3738.
[31] SERAYDARIAN, R.P., BURRELL, K.H., GROEBNER, R.J., Rev. Sci. Instrum. **59** (1988) 1530.
[32] HEIDBRINK, W.W., KIM, Jinchoon, GROEBNER, R.J., Nucl. Fusion **28** (1988) 1897.
[33] JOHNSON, D., BELL, M., BITTER, M., et al., in Plasma Physics and Controlled Nuclear Fusion Research 1982 (Proc. 9th Int. Conf. Baltimore, 1982), Vol. 1, IAEA, Vienna (1983) 9.
[34] LAO, L.L., St. JOHN, H., STAMBAUGH, R.D., KELLMAN, A.G., PFEIFFER, W.W., Nucl. Fusion **25** (1985) 1611.
[35] HEIDBRINK, W.W., SAGER, G., Nucl. Fusion **30** (1990) 1015.
[36] St. JOHN, H., HARVEY, R.W., MARCUS, F.B., ARMENTROUT, C.J., BRAMSON, G., Bull. Am. Phys. Soc. **27** (1982) 1059.
[37] FU, G.Y., CHENG, C.Z., Phys. Fluids B **2** (1990) 985.
[38] SPONG, D.A., HOLMES, J.A., LEBOEUF, J.-N., CHRISTENSON, P.J., Fusion Technol. **18** (1990) 496.
[39] HEIDBRINK, W.W., KAITA, R., TAKAHASHI, H., GAMMEL, G., HAMMETT, G.W., KAYE, S., Phys. Fluids **30** (1987) 1839.
[40] WEILAND, J., CHEN, L., Phys. Fluids **28** (1985) 1359.
[41] BIGLARI, H., CHEN, L., Phys. Fluids **29** (1986) 2960.
[42] CAMPBELL, R.B., A Study of Global Alfvén Eigenmodes Driven by Energetic Particles in the International Thermonuclear Experimental Reactor and Doublet III-D, Rep. LLNL-ITER-90-007, Lawrence Livermore National Laboratory, Livermore, CA (1990).
[43] CARNEVALI, A., SCOTT, S.D., NEILSON, G.H., GALLOWAY, M., STEVENS, P., THOMAS, C.E., Nucl. Fusion **28** (1988) 951.
[44] EQUIPE, TFR, in Plasma Physics and Controlled Nuclear Fusion Research 1986 (Proc. 11th Int. Conf. Kyoto, 1986), Vol. 1, IAEA, Vienna (1987) 179.
[45] GOLDSTON, R.J., KAITA, R., BEIERSDORFER, P., et al., Nucl. Fusion **27** (1987) 921.

(Manuscript received 11 February 1990
Final manuscript received 13 May 1991)